Homogeneous crystal nucleation in liquid copper under quasi-isentropic compression

Y. Cai, L. Wang, H. A. Wu, M. H. Zhu, C. L. Liu, and S. N. Luo

Homogeneous crystal nucleation in liquid Cu under quasi-isentropic compression

Y. Cai,[1,2] L. Wang,[2] H. A. Wu,[1,*] M. H. Zhu,[3,†] C. L. Liu,[4] and S. N. Luo[2,‡]

[1] *CAS Key Laboratory of Materials Behavior and Design, Department of Modern Mechanics,*

University of Science and Technology of China, Hefei, Anhui 230027, P. R. China

[2] *The Peac Institute of Multiscale Sciences,*

Chengdu, Sichuan 610031, P. R. China

[3] *Key Laboratory of Advanced Technologies of Materials,*

Ministry of Education, Southwest Jiaotong University,

Chengdu, Sichuan 610031, P. R. China

[4] *Institute of Fluid Physics, Mianyang, Sichuan 621900, P. R. China*

(Dated: June 25, 2015)

Abstract

Shock-induced freezing in liquids has long been a subject of interest as well as mystery. With large-scale molecular dynamics simulations, we demonstrate that homogeneous crystal nucleation in liquid Cu can be realized under certain supercooling (θ), via quasi-isentropic compression or ramp wave loading with a particle velocity u_{p} achieved within a ramp time τ. The simulations yield the τ–u_{p}–θ relations for homogeneous crystallization at the spatial and temporal scales of molecular dynamics; a ramp wave loading with $\tau \sim 100$ ps is essentially isentropic for liquid Cu. Based on classical nucleation theory, we predict θ, and thus u_{p}, as required for homogenous nucleation in experiments with larger length and time scales. Homogeneous nucleation can also be achieved with shock loading in initially sueprcooled liquids.

I. INTRODUCTION

The phenomenon of crystal nucleation and growth out of a liquid is ubiquitous, heavily studied but still not well understood.[1–6] Solidification under high strain-rate loading has long been a subject of particular interest.[7,8] Rapid crystallization may occur as a result of effective supercooling[9] via dynamic compression to high pressures. Experiments on solidification under single-shock loading were conducted on metallic and non-metallic liquids such as Bi and Sn,[10–14] H_2O,[15,16] CCl_4,[17] and C_6H_6.[18] Compared to shock compression, the temperature rise under quasi-isentropic or isentropic compression is much less,[19] thus advantageous for solidification. Quasi-isentropic compression experiments were recently carried out on Bi,[20] Sn,[21,22] and water.[23–25] Measurements with such diagnostics as laser velocimetry and high-speed photography suggest both homogeneous and heterogeneous crystallization during shock or quasi-isentropic compression.[7,23,24] Crystallization in liquid He under acoustic wave loading (μs time scale and <10 MPa) was observed based on index of refraction, light absorption or scattering measurements.[26,27] Nonetheless, the small temporal and spatial scales inherent in nucleation render experimental observations exceptionally challenging for dynamic extreme conditions (e.g., on the orders of 10 GPa and 100 GPa achieved within 10–100 ns).

While quasi-isentropic loading experiments have led to significant insights into solidification under dynamic extreme conditions, several key questions remain open even for simple liquids, including whether homogeneous nucleation can indeed occur during dynamic compression, and under what loading conditions (ramp time and loading strength) if it does; when a ramp wave loading can be deemed effectively isentropic. To address these questions, we choose a representative metallic liquid (Cu), and perform molecular dynamics (MD) simulations of solidification under ramp wave loading as well as shock loading. MD simulations have high spatial and temporal resolutions relevant to crystal nucleation,[28] and the simulation scales can be comparable to those in ultrafast loading experiments with fs–ns lasers.[29] We demonstrate homogeneous crystal nucleation in liquid Cu under quasi-isentropic loading, and predict the ramp time and loading strength for such nucleation during dynamic loading at larger spatial and temporal scales, based on MD simulations and classical nucleation theory. Shock loading of initially supercooled liquids can also lead to homogeneous crystallization.

II. METHODOLOGY

An accurate embedded-atom method potential[30] is used to describe the atomic interactions in Cu, and the Large-scale Atomic/Molecular Massively Parallel Simulator,[31] for MD simulations. We apply the constant pressure-temperature ensemble to obtain the initial liquid configurations under three-dimensional (3D) periodic boundary conditions. Several techniques such as forward flux sampling,[32] barrier crossing[32] and seeding methods[33] can be useful for obtaining nucleation rate, energy barrier or critical size in nucleation processes without applying brute force.[34] However, these methods are not applicable to dynamic loading involving wave propagation. Thus, we apply the piston method for ramp wave and shock simulations[35] with the microcanonical ensemble. In dynamic loading, periodic boundary condition is not applied along the wave propagation direction or the x-axis.

The system dimensions are approximately $1300 \times 8 \times 8$ nm^3 for ramp wave loading and $700 \times 11 \times 11$ nm^3 for shock wave loading, corresponding to $\sim$7 million atoms. Initially, Wave propagation is along the longest dimension or the x-axis, initially from left to right. The time step for integrating the equation of motion is 1 fs. One initial liquid configuration is equilibrated at 1325 K, i.e., the equilibrium melting temperature (T_{m}) of Cu at zero pressure.[36] We also obtain a liquid configuration at 1000 K for investigating crystallization in an initially supercooled liquid under shock wave loading, as opposed to ramp wave loading. Then, a small region on the left is set as the piston[35] consisting of liquid Cu atoms. The interactions between the piston and the rest of the atoms in the configuration are described with the same interatomic potential, while the atoms in the piston do not participate in molecular dynamics. Heterogeneous nucleation near the atomic piston does not occur in our simulations. A ramp wave is driven into liquid Cu by a moving atomic piston[35] with its velocity updated at each time step. The piston is accelerated from 0 to a terminal velocity, or subjected to a constant acceleration for ramp wave loading, while it is assigned a constant velocity for shock wave loading. We define the ramp time τ as the time required for a piston to reach a designated velocity, u_{p}. A ramp wave may develop into a shock during propagation.

We perform 1D binning analyses[37,38] to resolve spatially such physical properties as stress (σ_{ij}) and temperature (T) profiles along the wave propagation direction. The binning width is 5 Å. To calculate T and σ_{ij} within each bin, we need remove its center-of-mass velocity,

$\bar{v}_i$ ($i = x$, y and z), or apply corrections: $\Delta T = -(m/3k_{\mathrm{B}})(\bar{v}_x^2 + \bar{v}_y^2 + \bar{v}_z^2)$, and $\Delta\sigma_{ij} = -(Nm/V_{\mathrm{a}})\bar{v}_i\bar{v}_j$, where m is the atomic mass, V_{a} is the atomic volume, N is the number of Cu atoms in the volume under consideration, and k_{B} is Boltzmann's constant.

We characterize the local structure around an atom with the common neighbor analysis (CNA).[39,40] Structure changes upon crystallization are also described with 2D X-ray diffraction (XRD).[28,41] In XRD, the scattered intensity $I(\mathbf{k})$ is

$$I(\mathbf{k}) = \frac{F(\mathbf{k})F^*(\mathbf{k})}{N}, \tag{1}$$

where the structure factor

$$F(\mathbf{k}) = \sum_{j=1}^{N} f_j \exp(2\pi i \mathbf{k} \cdot \mathbf{r}_j). \tag{2}$$

Here $\mathbf{k}$ is the reciprocal space vector, and $\mathbf{r}$ is the position of an atom in the real space; f is the atomic scattering factor for photons. For a wavelength λ, the diffraction angle θ and $\mathbf{k}$ are related via Bragg's law

$$\frac{2\sin\theta}{\lambda} = \frac{1}{d_{hkl}} = |\mathbf{k}|, \tag{3}$$

where d represents the d-spacing between (hkl) planes. We use $\lambda = 1.54$ Å (8.05 keV), corresponding to Cu K$_\alpha$ radiation, in XRD simulations.

III. RESULTS AND DISCUSSION

Shock and isentropic compression represent two extremes, and ramp wave loading is intermediate between them. To investigate solidification induced by dynamic compression, we first calculate pressure (P) and temperature on the isentrope and Hugoniot centered at zero pressure and 1325 K. The isentrope is obtained via thermodynamic integration[7]

$$\int_{T_0}^{T_S} \frac{\mathrm{d}T}{T} = \int_{V_0}^{V} -\gamma\frac{\mathrm{d}V}{V}. \tag{4}$$

Here, V is specific volume, γ is the Grüneisen parameter, and subscripts 0 and S refer to the initial state and isentrope, respectively. Numerical integration is based on a (P, V, T, E) dataset acquired from numerous MD runs with a system size of $\sim$500000 atoms under constant volume-temperature ensemble (E: internal energy).

The Hugoniot states of liquid Cu are obtained directly from MD simulations at different shock strengths. Shock loading involves an increase in entropy (S), so Hugoniot $P_{\mathrm{H}}(V)$ is
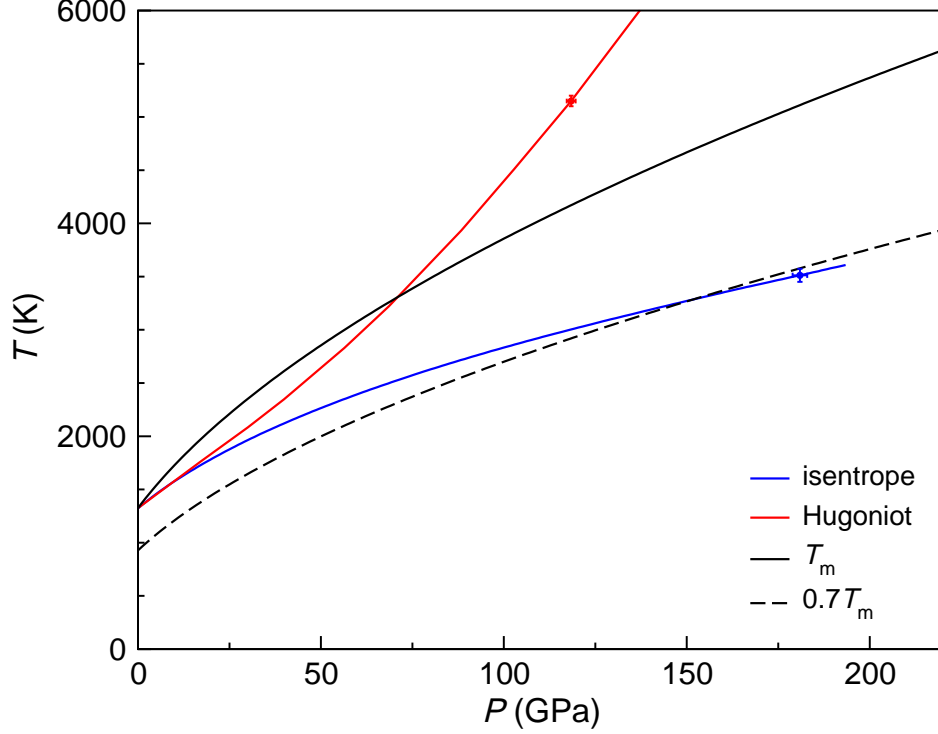
4

FIG. 1. The equilibrium melting curve $T_m(P)$, a supercooling curve $0.7T_m(P)$, and the liquid Hugoniot and isentrope centered at 1325 K and 0 GPa. The uncertainties in P and T on the Hugoniot and isentrope are exemplified by the dots with error bars.

steeper than isentrope $P_S(V)$, and

$$\left(-\frac{dP}{dV}\right)_H - \left(-\frac{dP}{dV}\right)_S = \frac{\gamma T}{V}\left(-\frac{dS}{dV}\right)_H \gtrsim 0, \tag{5}$$

where subscript H denotes Hugoniot. Consequently, $V_H \gtrsim V_S$ at the same pressure as a result of thermal expansion, i.e., $T_H(P) \gtrsim T_S(P)$.[7] Thus, crystallization is more difficult on the Hugoniot than on the isentrope for a given pressure.

The calculated isentrope and Hugoniot centered at 1325 K and zero pressure are shown in Fig. 1 along with the equilibrium melting curve, $T_m(P)$,[36] and a supercooling curve $(0.7T_m)$. Indeed, the isentrope lies below the Hugoniot and $T_m(P)$, and concaves downward, while the Hugoniot is below $T_m(P)$ at low pressures and then rises above it at $P > 71$ GPa, concaving upward.

Homogeneous nucleation is of interest for compression-induced solidification, but requires a certain amount of supercooling, $\theta = (1 - T/T_m)|_P$, given a finite time window of observation and finite system size. In MD temporal and spatial scales, homogeneous nucleation
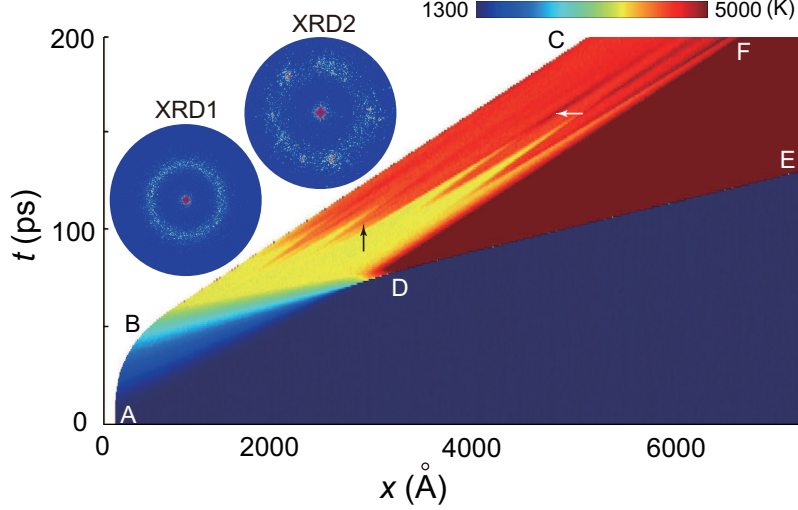
FIG. 2. x–t diagram in terms of temperature for ramp wave loading. Insets XRD1 and XRD2 are X-ray diffraction patterns from the (quasi-)isentropic compression region at 0 ps and 170 ps, respectively. The initial system dimensions are $1300 \times 8 \times 8$ nm^3.

occurs at $\theta \approx 0.3$ or $T \approx 0.7T_\mathrm{m}$, regardless of pressure.[36,42] With increasing pressure, supercooling increases on the isentrope, which intersects the supercooling curve $0.7T_\mathrm{m}(P)$ at ~152 GPa. However, the maximum supercooling on the Hugoniot is only 0.11 at 27 GPa, and θ decreases at higher pressures. Thus, shock-induced solidification in liquid Cu with initial temperature of 1325 K appears unlikely at MD scales, in contrast to isentropic compression. Pure isentropic compression is not realistic for dynamic compression, and can only be approached by ramp wave or quasi-isentropic loading with sufficiently long ramp time τ. We explore below different ramp wave and shock loadings, and discussions refer to the initial conditions of 1325 K and zero pressure unless stated otherwise.

As an example, Figure 2 shows the position–time (x–t) diagram in terms of temperature for ramp wave loading of liquid Cu, where the piston follows trajectory ABC with a terminal velocity $u_\mathrm{p} = 3$ km/s achieved within 60 ps. At D, the perturbations develop into a shock DE. Two regions are identified with a drastic difference in temperature: (quasi-)isentropic compression ($ABCFD$), and shock-compression (DEF). As expected, shock heating is much more pronounced than (quasi-)isentropic heating.

In the (quasi-)isentropic compression region, nuclei of different sizes at random locations are observed (arrows, 70 ps, Fig. 3), indicating homogeneous nucleation. On the contrary, nucleation is absent in the shock compression region (regions behind the red dashed line
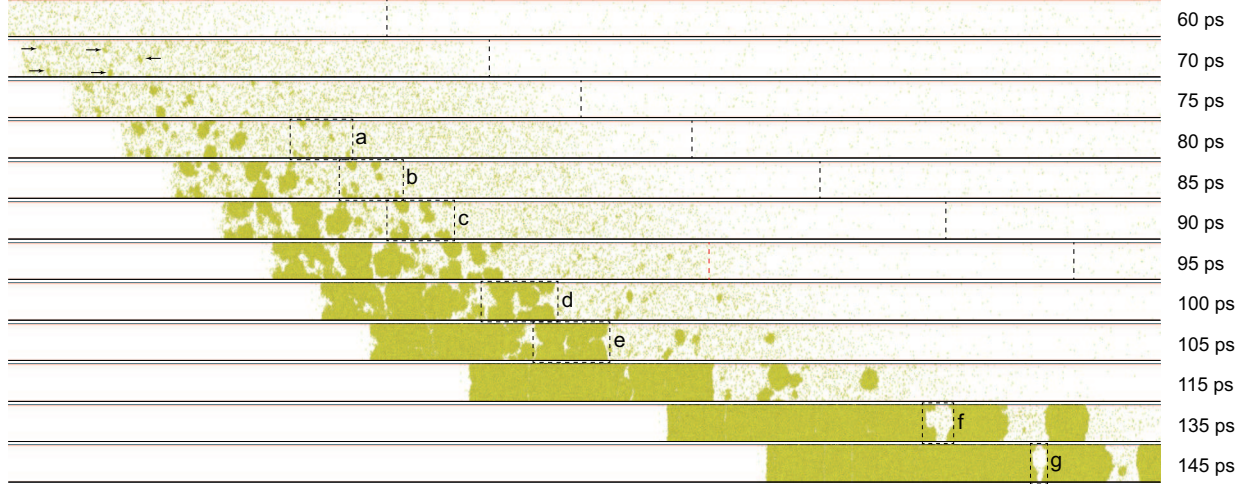
FIG. 3. Snapshots of homogeneous crystal nucleation and growth during ramp wave loading. Only "solid-like" atoms (via common neighbor analysis) are plotted. The dashed lines denote the boundary between the quasi-isentropic and shock compression zone (red), and wave fronts (black). Regions a–e refer to independent nucleation and growth followed by coalescence of nuclei, while regions f and g show interface growth. Regions e and g correspond to those indicated by the arrows in Fig. 2. The initial system dimensions are $1300 \times 8 \times 8$ nm^3.

in Fig. 3) with much higher temperatures (corresponding to DEF in Fig. 2). The atomic piston appears to have negligible effect on nucleation. Figure 3 shows that crystal nuclei grow independently into quasi-spheres at early stages (regions a–c) and then coalesce (regions d and e), leading to local temperature rise due to the release of latent heat ("self" heating; black arrow, Fig. 2). At later stages, crystallization proceeds from the solid-liquid interfaces (surface growth, regions f and g in Fig. 3) and releases latent heat into the adjacent liquid, forming high temperature stripes within the solidifying region (conduction heating; white arrow in Fig. 2), while the shock compression region shows no heterogeneities expected for homogeneous nucleation.

In order to confirm crystallization, we compute 2D XRD patterns for the (quasi-)isentropic compression region at different time (Fig. 2 insets XRD1 and XRD2). At $t = 0$ ps, only a broad, diffuse, Debye-Scherrer ring for liquid Cu is observed. At 170 ps, several {111} and {200} diffraction spots appear randomly on the diffuse diffraction ring, and the diffraction angles move outward, indicating crystallization under compression.

There are different ways to accelerate the piston for ramp wave loading, and linear accel-
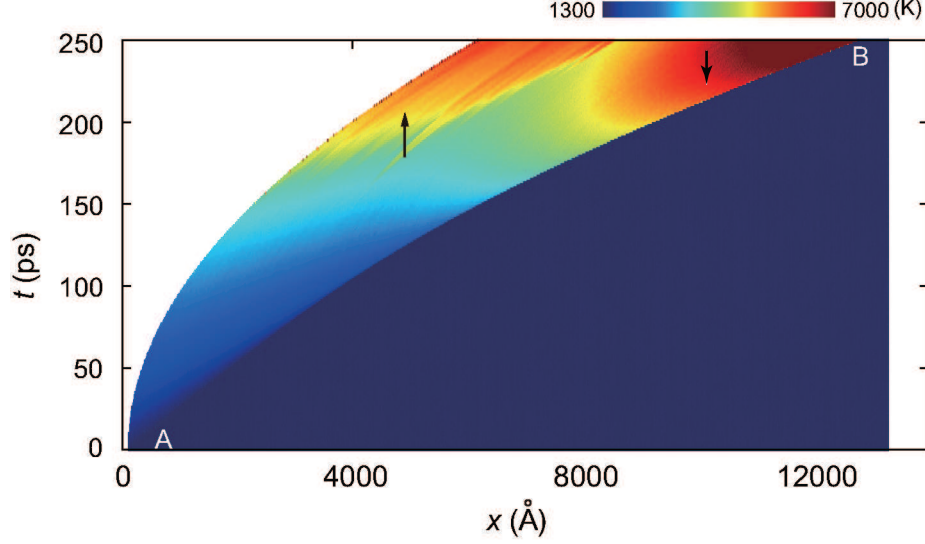
FIG. 4. x–t diagram for ramp wave loading with a linear acceleration. Color-coding is based on temperature. Crystallization occurs in the upward arrowed region. The initial system dimensions are $1300 \times 8 \times 8$ nm^3.

eration is a simplest one for understanding underlying mechanisms. One ramp wave loading case of linear acceleration is illustrated with the x–t diagram in Fig. 4. Homogeneous crystal nucleation occurs on the piston side, and the growth of the nuclei leads to local temperature rise, indicated by the upward arrow. The nucleation and growth manifest initially as independent streaks in Fig. 4. The temperature gradient across the wavefront AB increases as its propagation proceeds, and this steepening gives rise to a high temperature zone immediately behind it (indicated by the downward arrow).

Figure 5 shows in more detail the evolutions of particle velocity u, θ, P and T for the linear acceleration case in Fig. 4. The $u_x(x)$ profiles [Fig. 5(a)] exhibit dynamic wavefront steepening, leading to the formation of a well-defined shock at $t = 140$ ps; the shock becomes stronger and faster with increasing time. On the piston side, supercooling increases with increasing particle velocity or pressure [Fig. 5(b)]. However, the increasing shock strength leads to an increase in temperature, and a decrease in supercooling to zero and even negative values near the shock front [Figs. 5(b) and 5(c)]. At $t \leq 100$ ps, the compression is essentially isentropic [Fig. 5(c)], despite the formation of weak shocks (the Hugoniot and isentrope coincide at low pressures). At later stages, the states in the region immediately behind the shock front deviate from the isentrope and approach the Hugoniot. The lowest-
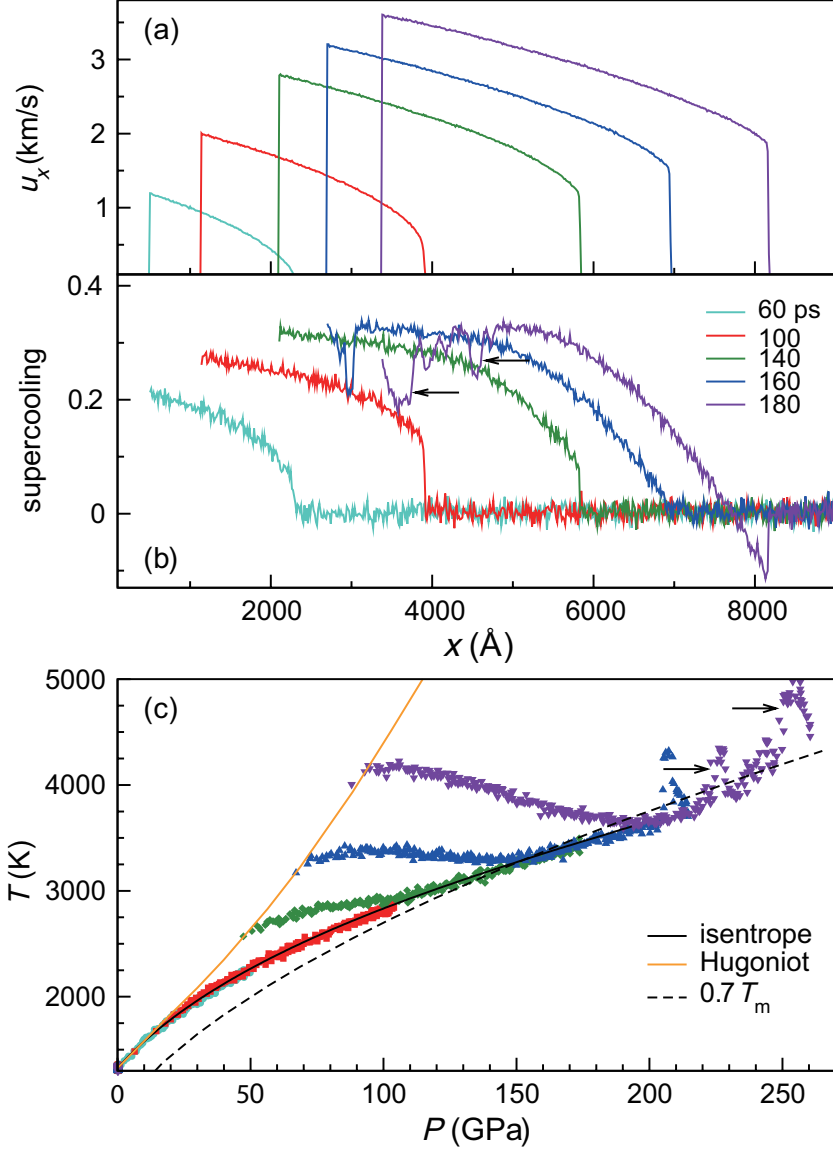
8

FIG. 5. Profiles of particle velocity (a) and supercooling (b) at different time for linearly accelerated piston, and the corresponding P–T plots (c). Loading direction in (a) and (b): left $\rightarrow$ right. The initial system dimensions are $1300 \times 8 \times 8$ nm^3.

pressure states on the shock front side are on the Hugoniot, the highest-pressure states on the piston side remain on the isentrope, and the intermediate-pressure states, lying between the Hugoniot and isentrope, are quasi-isentropic [Fig. 5(c)].

With increasing pressure (or u_p) on the ramp, supercooling and thus the driving force for crystallization increases. When supercooling exceeds ~ 0.3 (140 ps), homogeneous nucleation and growth occur first in the isentropically compressed region, and crystallization may grow
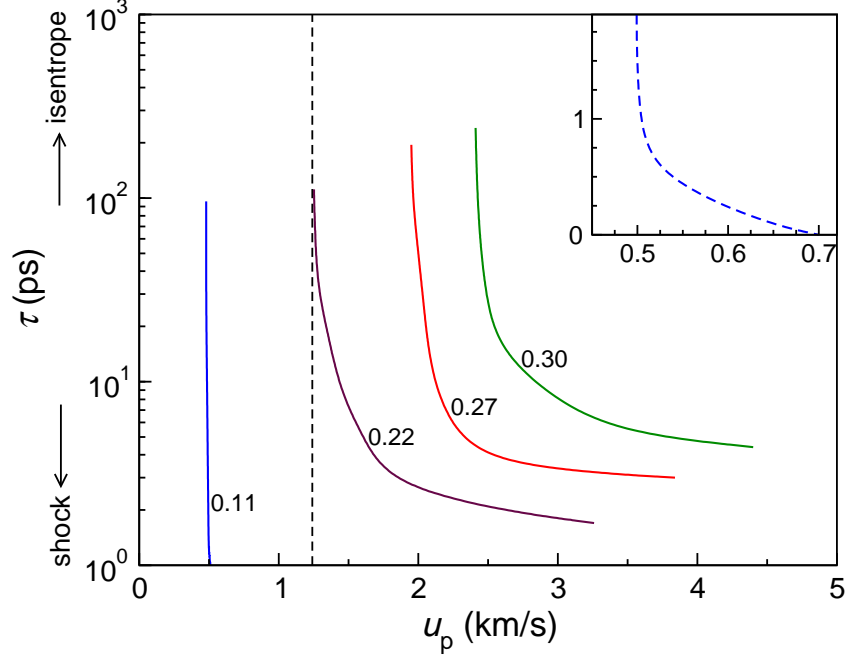
9

FIG. 6. Iso-supercooling curves on the τ–u_{p} plane, for ramp wave loading with a linearly accelerated piston. The inset shows the curve for $\theta = 0.11$ at small τ, extrapolated to $\tau = 0$. The dashed line denotes the asymptotic value of u_{p} when an iso-supercooling curve approaching the isentrope.

into the quasi-isentropically compressed region; subsequently, the release of latent heat leads to local temperature rise and the reduction of supercooling [e.g., the arrows at 160 ps and 180 ps, Figs. 5(b) and 5(c)].

For a given linear acceleration (a), it takes a ramp time τ to achieve certain $u_{\mathrm{p}} = \tau a$; the largest supercooling is recorded, and we thus obtain $(\tau, u_{\mathrm{p}}, \theta)$ triplets. Ramp wave loading with different linear accelerations is conducted, and the iso-θ curves are plotted in Fig. 6. Each point on such a curve denotes the required ramp time τ to reach piston velocity u_{p} and achieve a prescribed supercooling θ.

For given τ, larger u_{p} leads to larger supercooling, while for given u_{p}, decreasing or increasing ramp time shifts the loading towards shock or isentropic compression. For large θ, the iso-θ curves are essentially parallel to the x-axis at high u_{p}. Only small-θ curves intersect the x-axis at low u_{p} ($\tau = 0$), e.g., $\theta \sim 0.11$ for an ideal shock at 0.7 km/s (Fig. 6 inset), which also represents the maximum supercooling achievable on the principal Hugoniot (Fig. 1). Decreasing τ towards zero leads to an extremely narrow region undergoing isentropic or quasi-isentropic compression. On the other hand, the iso-θ curves steepen up rapidly as τ

increases, e.g., above 100 ps (the dashed line), and further increasing τ is not efficient in reducing shock strength for given θ. A ramp wave loading with $\tau \sim 100$ ps is essentially isentropic. However, a longer ramp time does increase the isentropically compressed zone, and therefore, the total volume of crystallization.

Different experimental conditions, e.g., different loading devices and sample sizes, require different θ, and consequently, different τ and u_{p} for homogeneous nucleation to occur. In order to predict u_{p} for homogeneous crystallization under given experimental conditions including τ, we calculate the corresponding supercooling from MD results (Fig. 6 and other known parameters) based on classical nucleation theory. The probability p for a given amount of parent phase containing no new phase[3] can be estimated as

$$p = \exp\left\{-\int I_0 \exp\left[f(\theta(\mathbf{r};t))\right]\mathcal{A}\mathrm{d}l\mathrm{d}t\right\}. \tag{6}$$

Here $f(\theta) = \beta[\theta^2(1-\theta)]^{-1}$, and $\beta = \frac{16\pi\gamma^3}{3\Delta H_{\mathrm{m}}k_{\mathrm{B}}T_{\mathrm{m}}}$ is the dimensionless nucleation barrier characteristic of a material (γ is the solid-liquid interfacial energy, and ΔH_{m} is the heat of fusion),[9,36,42] I_0 is a prefactor, $\mathcal{A}$ is the cross-sectional area along the loading direction, and l is the thickness of a supercooled slab under consideration. Supercooling θ is a function of position ($\mathbf{r}$) and t. Since nucleation rate near a critical supercooling (subscript c) is predominant,[2,42] Eq. (6) is reduced to Eq. (7) using the corresponding "critical" values, we have

$$p \sim \exp\left\{-I_0\exp\left[-\frac{\beta}{\theta_{\mathrm{c}}^2(1-\theta_{\mathrm{c}})}\right]\mathcal{A}l_{\mathrm{c}}t_{\mathrm{c}}\right\}. \tag{7}$$

Here l_{c} is approximately proportional to ramp time τ; t_{c} is the duration of sustained supercooling, and scales with the sample dimension d_x along the x-axis. Assuming the same p for different system sizes and τ, Eq. (7) allows one to estimate the required supercooling via

$$\frac{\exp\left\{-\frac{\beta}{\theta_{\mathrm{c1}}^2(1-\theta_{\mathrm{c1}})}\right\}}{\exp\left\{-\frac{\beta}{\theta_{\mathrm{c2}}^2(1-\theta_{\mathrm{c2}})}\right\}} = \frac{\mathcal{A}_2 l_{\mathrm{c2}}\tau_{\mathrm{c2}}}{\mathcal{A}_1 l_{\mathrm{c1}}\tau_{\mathrm{c1}}}, \tag{8}$$

where subscripts 1 and 2 denote two different experimental or simulation scenarios. Given parameters from Ref. 36 and 42, $\theta = 0.3$ as in our MD simulations ($\mathcal{A} = 8 \times 8$ nm^2, $\tau_{\mathrm{c}} = 60$ ps, and $d_x = 1.3$ μm) corresponds to $\theta \sim 0.2$ for a sample size of $0.1 \times 1 \times 1$ cm^3 and $\tau = 1$ ns, i.e., homogeneous nucleation can be achieved in experiments on liquid Cu with ramp loading to $u_{\mathrm{p}} = 1.1$ km/s within a ramp time of 1 ns (Fig. 6) for such macroscopic dimensions.
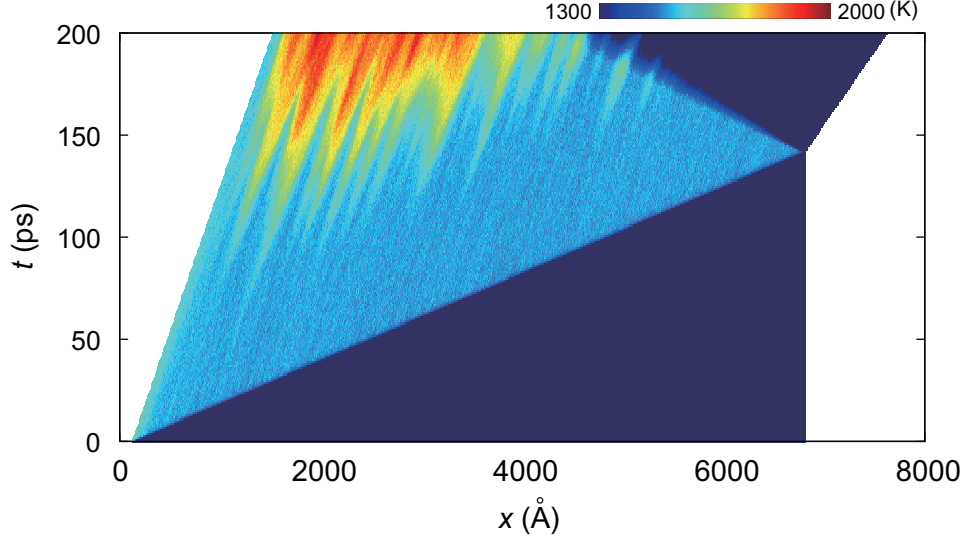
FIG. 7. x–t diagram for shock loading at $u_{\mathrm{p}} = 0.7$ km/s, showing shock-induced crystallization of a liquid initially at a supercooled state. Color-coding is based on temperature. The initial system dimensions are $700 \times 11 \times 11$ nm^3.

Although shock-induced solidification appears unlikely at MD simulation scales for liquid Cu initially at or above the equilibrium melting temperature at zero pressure, it would be desirable to investigate shock-induced crystallization in initially supercooled Cu liquids. As an example, we examine liquid Cu initially supercooled to 1000 K ($\theta \sim 0.24$). Figure 7 shows the corresponding x–t diagram in terms of temperature for shock loading with a particle velocity of 0.7 km/s. The transient supercooling behind the shock front is approximately 0.33, which is sufficient for homogeneous nucleation at MD scales. Thus, the initial supercooling offsets partially shock-induced heating, similar to the mitigation in heating by (quasi-)isentropic compression. For comparison, the maximum supercooling on the principal Hugoniot centered at 1325 K and zero pressure is only 0.11 (Fig. 1).

Individual high temperature streaks form in the whole shocked region (Fig. 7) via homogeneous nucleation and growth, which are accompanied by the release of latent heat upon crystallization. These streaks coalesce at later stages as growth proceeds. Note that the shock front leads the crystallization "front" by 10–150 ps, since a finite incubation time is required for homogeneous nucleation. The incubation time varies for different locations (another manifestation of homogeneous nucleation), because nucleation events heavily depend on thermal fluctuations.[28,43] However, crystallization does not yield sufficient perturbations

in particle velocity to form a phase change "shock," since the liquid and solid are indistinguishable in the shock velocity–particle velocity plots for Cu as demonstrated in experiments and simulations.[36,44]

IV. CONCLUSION

Homogeneous crystal nucleation is demonstrated for liquid Cu under dynamic compression, via effective supercooling induced by ramp wave or (quasi-)isentropic loading. We obtain the τ–u_{p}–θ relations for homogeneous crystallization at the MD time and length scales; a ramp wave loading with $\tau \sim 100$ ps is essentially isentropic for liquid Cu. We predict θ, and thus u_{p}, for achieving homogenous nucleation at larger temporal and spatial scales (ns and mm), in experiments on liquid Cu and likely other liquids. On the other hand, homogeneous nucleation can also be achieved with shock loading in initially supercooled liquid Cu.

* wuha@ustc.edu.cn

† zhuminhao@swjtu.cn

‡ sluo@pims.ac.cn

[1] B. J. Alder and T. E. Wainwright, J. Chem. Phys. **31**, 459 (1959).

[2] J. W. Christian, *The Theory of Transformation in Metals and Alloys* (Pergaman, New York, 1965).

[3] K. F. Kelton, Solid State Phys. **45**, 75 (1991).

[4] B. O'Malley and I. Snook, Phys. Rev. Lett. **90**, 085702 (2003).

[5] D. Moroni, P. ten Wolde, and P. Bolhuis, Phys. Rev. Lett. **94**, 235703 (2005).

[6] F. H. Streitz, J. N. Glosli, and M. V. Patel, Phys. Rev. Lett. **95**, 225701 (2006).

[7] G. E. Duvall and R. A. Graham, Rev. Mod. Phys. **49**, 523 (1977).

⁸ A. I. Funtikov, High Temp. **49**, 439 (2011).

⁹ S. N. Luo, A. Strachan, and D. C. Swift, J. Chem. Phys. **120**, 11640 (2004).

¹⁰ R. F. Duff and F. S. Minsall, Phys. Rev. **108**, 1207 (1957).

¹¹ J. R. Asay, J. Appl. Phys. **45**, 4441 (1974).

¹² K. V. Volkov and V. A. Sibilev, Prikl. Mekh. Tekh. Fiz **4**, 125 (1981).

¹³ J. D. Colvin, B. W. Reed, A. F. Jankowski, M. Kumar, D. L. Paisley, D. C. Swift, T. E. Tierney, and A. M. Frank, J. Appl. Phys. **101**, 084906 (2007).

¹⁴ J. D. Colvin, A. F. Jankowski, M. Kumar, W. J. M. Chan, B. W. Reed, D. L. Paisley, and T. E. Tierney, J. Appl. Phys. **105**, 014902 (2009).

¹⁵ J. M. Walsh and M. H. Rice, J. Chem. Phys. **26**, 815 (1957).

¹⁶ A. P. Rybakov and I. A. Rybakov, Eur. J. Mech. B **14**, 323 (1995).

¹⁷ P. C. Lysne, J. Chem. Phys. **55**, 5242 (1971).

¹⁸ A. Matsuda, K. Kondo, and K. G. Nakamura, J. Chem. Phys. **124**, 054501 (2006).

¹⁹ L. Davison and R. A. Graham, Phys. Reports **55**, 255 (1979).

²⁰ F. H. Streitz, J. H. Nguyen, D. Orlikowski, R. Minich, J. A. Moriarty, and N. C. Holmes, Tech. Rep. 02-ERD-033, Lawrence Livermore National Laboratory (2005).

²¹ D. B. Reisman, A. Toor, R. C. Cauble, C. A. Hall, J. R. Asay, M. D. Knudson, and M. D. Furnish, J. Appl. Phys. **89**, 1625 (2001).

²² J. P. Davis, D. B. Hayes, J. R. Asay, P. W. Watts, P. A. Flores, and D. B. Reisman, AIP Conference Proceedings **620**, 221 (2002).

²³ D. H. Dolan and Y. M. Gupta, J. Chem. Phys. **121**, 9050 (2004).

²⁴ D. H. Dolan, M. D. Knudson, C. A. Hall, and C. Deeney, Nat. Phys. **3**, 342 (2007).

²⁵ M. Bastea, S. Bastea, J. E. Reaugh, and D. B. Reisman, Phys. Rev. B **75**, 172104 (2007).

²⁶ X. Chavanne, S. Balibar, and F. Caupin, Phys. Rev. Lett. **86**, 5506 (2001).

²⁷ R. Ishiguro, F. Caupin, and S. Balibar, Europhys. Lett. **75**, 91 (2006).

²⁸ J. C. E, L. Wang, Y. Cai, H. A. Wu, and S. N. Luo, J. Chem. Phys. **142**, 064704 (2015).

²⁹ D. H. Kalantar, J. F. Belak, G. W. Collins, J. D. Colvin, H. M. Davies, J. H. Eggert, T. C. Germann, J. Hawreliak, B. L. Holian, K. Kadau, et al., Phys. Rev. Lett. **95**, 075502 (2005).

³⁰ Y. Mishin, M. J. Mehl, D. A. Papaconstantopoulos, A. F. Voter, and J. D. Kress, Phys. Rev. B **63**, 224106 (2001).

³¹ S. Plimpton, J. Comput. Phys. **117**, 1 (1995).

[32] C. Valeriani, E. Sanz, and D. Frenkel, J. Chem. Phys. **122**, 194501 (2005).

[33] E. Sanz, C. Vega, J. R. Espinosa, R. Caballero-Bernal, J. L. F. Abascal, and C. Valeriani, J. Am. Chem. Soc. **135**, 15008 (2013).

[34] E. B. Moore and V. Molinero, Nature **479**, 506 (2011).

[35] B. L. Holian, Shock Waves **5**, 149 (1995).

[36] Q. An, S. N. Luo, L. B. Han, L. Zheng, and O. Tschauner, J. Phys.: Condens. Matter **20**, 095220 (2008).

[37] S. N. Luo, Q. An, T. C. Germann, and L. B. Han, J. Appl. Phys. **106**, 013502 (2009).

[38] S. N. Luo, T. C. Germann, T. G. Desai, D. L. Tonks, and Q. An, J. Appl. Phys. **107**, 123507 (2010).

[39] D. Faken and H. Jnsson, Comput. Mater. Sci. **2**, 279 (1994), ISSN 0927-0256.

[40] H. Tsuzuki, P. S. Branicio, and J. P. Rino, Comput. Phys. Comm. **177**, 518 (2007).

[41] L. Wang, J. C. E, Y. Cai, F. Zhao, D. Fan, and S. N. Luo, J. Appl. Phys. **117**, 084301 (2015).

[42] S. N. Luo, T. J. Ahrens, T. Çağın, A. Strachan, W. A. Goddard III, and D. C. Swift, Phys. Rev. B **68**, 134206 (2003).

[43] L. Q. Zheng, Q. An, Y. Xie, Z. H. Sun, and S. N. Luo, J. Chem. Phys. **127**, 164503 (2007).

[44] S. P. Marsh, *LASL Shock Hugoniot Data* (University of California Press, Berkely, 1980).